ISSN 0021-3640, JETP Letters, 2019, Vol. 110, No. 11, pp. 755–759. © Pleiades Publishing, Inc., 2019.
Russian Text © The Author(s), 2019, published in Pis'ma v Zhurnal Eksperimental'noi i Teoreticheskoi Fiziki, 2019, Vol. 110, No. 11, pp. 759–764.

MISCELLANEOUS

Optical and Structural Phenomena at Multipulse Interference Femtosecond Laser Fabrication of Metasurfaces on a Thin Film of Amorphous Silicon

S. I. Kudryashov[a, b, *], P. A. Danilov[a, b], A. P. Porfirev[c, d], A. A. Rudenko[a], N. N. Melnik[a], A. A. Kuchmizhak[b, e], O. B. Vitrik[b, e], and A. A. Ionin[a]

[a] *Lebedev Physical Institute, Russian Academy of Sciences, Moscow, 119991 Russia*
[b] *Far Eastern Federal University, Vladivostok, 690041 Russia*
[c] *Institute of Image Processing Systems, Federal Research Center Crystallography and Photonics, Russian Academy of Sciences, Samara, 443001 Russia*
[d] *Korolev State Aerospace University, Samara, 443086 Russia*
[e] *Institute of Automation and Control Processes, Far Eastern Branch, Russian Academy of Sciences, Vladivostok, 690041 Russia*
**e-mail: kudryashovsi@lebedev.ru*

Received October 23, 2019; revised November 6, 2019; accepted November 6, 2019

The formation of hexagonal microarrays of nanoholes (metasurfaces) in a 50-nm hydrogenated amorphous silicon film by means of three-beam interference of femtosecond laser pulses of the visible range (wavelength 515 nm) is studied experimentally with various exposures of the film. Characterization of arrays by scanning electron and optical microscopy, as well as optical transmission and reflection microspectroscopy, shows that an increase in the number of fixed energy laser pulses leads to a gradual evaporative formation of nanoholes in the film and, overall, the metasurface. Raman microspectroscopy reveals a simultaneous growth of the volume content of the crystal phase.

DOI: 10.1134/S0021364019230103

1. Hydrogenated amorphous silicon (a-Si) with a transparency band in the optical range (>400 nm) is considered as a promising material for creating optical waveguides with low losses [1], connectors (interconnectors) [2], nonlinear optical devices of ultrafast switching [3], and structural nanoelements of metasurfaces [4]. Currently, optical and a-Si based nonlinear optical devices are formed by the combined method of sputtering and lithography, which is compatible with CMOS (complementary metal–oxide–semiconductor) technology of constructing integrated circuits and the related circuitry. However, this method has disadvantages, including high cost, significant levels of chemical contaminants, and lack of flexibility. On the other hand, high-performance laser nanostructuring microtechnologies have been actively developed in recent years [5–8], which make it possible to form large arrays of complex-shaped plasmon microelements in a reasonable time under precisely targeted exposure to femtosecond laser pulses with a high repetition rate. At the same time, the physical principles of femtosecond laser fabrication of single dielectric microelements [9, 10] and their large arrays, including the interaction of radiation with matter [11, 12] and related technical problems, are still under active development. In particular, in the case of a-Si films under multipulse action, the hindering factors are undesirable structural modification (e.g., crystallization) and subablative destruction/nanostructuring of films and individual nanoelements by the sections of a laser beam having a subablative energy density [13, 14], heat-induced destruction of dielectric nanoelements, and other factors that have yet to be established.

In this work, the experimental conditions for the formation in an amorphous silicon film of large ordered arrays of nanoholes (metasurfaces) in the spatial field created by the interference of three space-multiplexed and time-synchronized femtosecond laser pulses are investigated for the first time using optical and structural methods.

2. Multipulse three-beam interference nanostructuring of amorphous silicon (a-Si) films on glass slides placed on a three-coordinate motorized platform was performed using an optical scheme shown in Fig. 1a. The radiation source was ultrashort (FWHM duration of 0.3 ps) pulses of a visible range fiber laser (central wavelength of 515 nm). Pulses of the TEM_{00} mode were multiplexed into a hexagonal structure by a

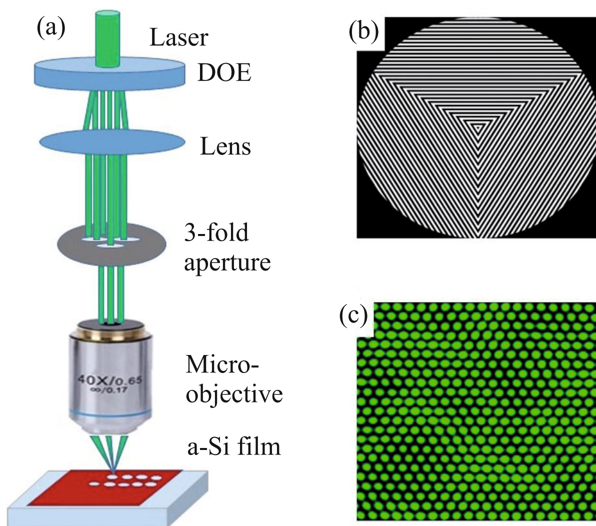

Fig. 1. (Color online) (a) Optical block diagram of a setup for three-beam interference recording of metasurfaces with multiplexing of a femtosecond laser pulse by a diffraction optical element. (b) Phase profile of a binary diffraction optical element for multiplexing laser radiation. (c) Experimental distribution of the radiation intensity in the scheme of three-beam interference.

binary diffraction optical element based on fused quartz (Figs. 1b, 1c). Further, the three extra beams were cut off by a diaphragm, and the remaining beams were focused on the silicon film by a microlens with a numerical aperture of NA = 0.65 (Fig. 1a). The three-beam interference was recorded on fresh sections of the film at a fixed maximum energy of the initial pulses of about 3 μJ and a variable exposure of $N = (1–5) \times 10^3$ pulses.

Hydrogenated a-Si films with a thickness of 50 nm were sprayed from gaseous monosilane on glass slides by the plasma-chemical method at a temperature of 800 K. Raman spectra (Fig. 2a) measured at room temperature at an exciting laser wavelength of 488 nm using an U-1000 microscope (Jobin Yvon) show the main known band of a-Si near 475 cm^{-1} (broadened TO band [15]). Measurements of transmission spectra in the range of 350–600 nm using an SF-2000 spectrophotometer revealed a fast growth of the film transmittance in the range of 400–500 nm with an interference minimum of transmission and an interference maximum of reflection near 400 nm (Fig. 2b), as well as high absorption of ultrashort pulses at a wavelength of 515 nm with an absorption coefficient of $\alpha(515\text{nm}) \approx 4 \times 10^5$ cm^{-1}. Preliminary visualization of arrays of nanoholes in a-Si films was carried out using an Altami-6 optical microscope, and more detailed studies of the structure of the arrays were carried out using a JEOL 7001F scanning electron microscope. A MFUK microscope–spectrometer was used for optical transmittance and reflectance microspectroscopy of the arrays in the range of 400–900 nm including both the entire array (area of about 25 μm for the aperture size of 500 μm and a 20× microlens) and individual cells (area about 2.5 μm for the aperture size 100 μm, and a 40× microlens).

3. The exposure of the 50-nm a-Si film to three interfering beams with a small number of pulses N = 1–10 leads to the formation of a hexagonal array of both nanocraters and through nanoholes with a diameter of 300–500 nm (Figs. 3, 4). This is due to the incomplete spatial homogeneity of the interference pattern associated mainly with some imperfection of the spatial transverse alignment of the used simple optical scheme; the inhomogeneity of the profile of the original TEM_{00} mode also plays a role. As the exposure is increased to N = 50–100, through nanoholes appear almost everywhere in the interference region, while a structure period of about 1.5 μm is preserved (Fig. 3); the low rate of hole formation indicates a slow evaporative removal of the film in spite of its relatively small thickness. Further, when $N > 500$,

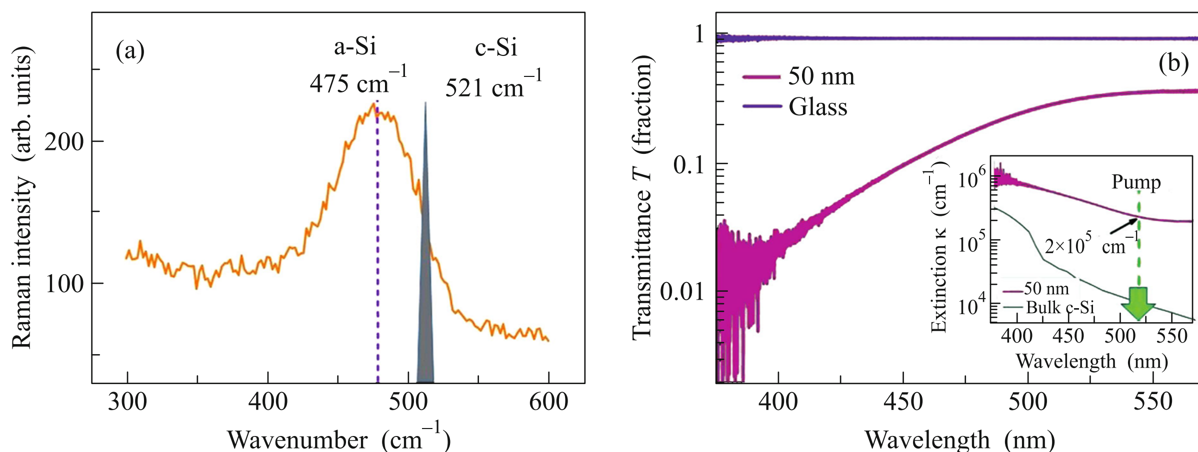

Fig. 2. (Color online) (a) Raman spectrum of an a-Si film 50 nm thick. (b) Transmission spectra and extinction coefficient (inset) of the same a-Si film.

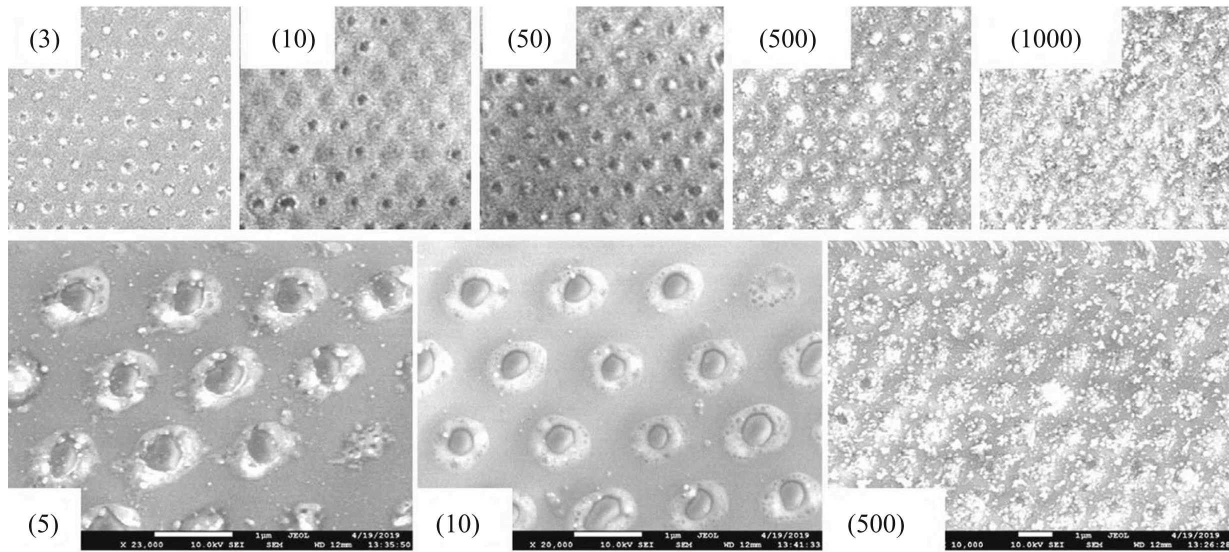

Fig. 3. Scanning electron microscopy images of arrays of nanoholes in an a-Si film 50 nm thick at exposures of (top row) 3–1000 pulses (image size 10 × 10 μm) and (bottom row) 3, 10, and 500 pulses (size label corresponds to 1 μm).

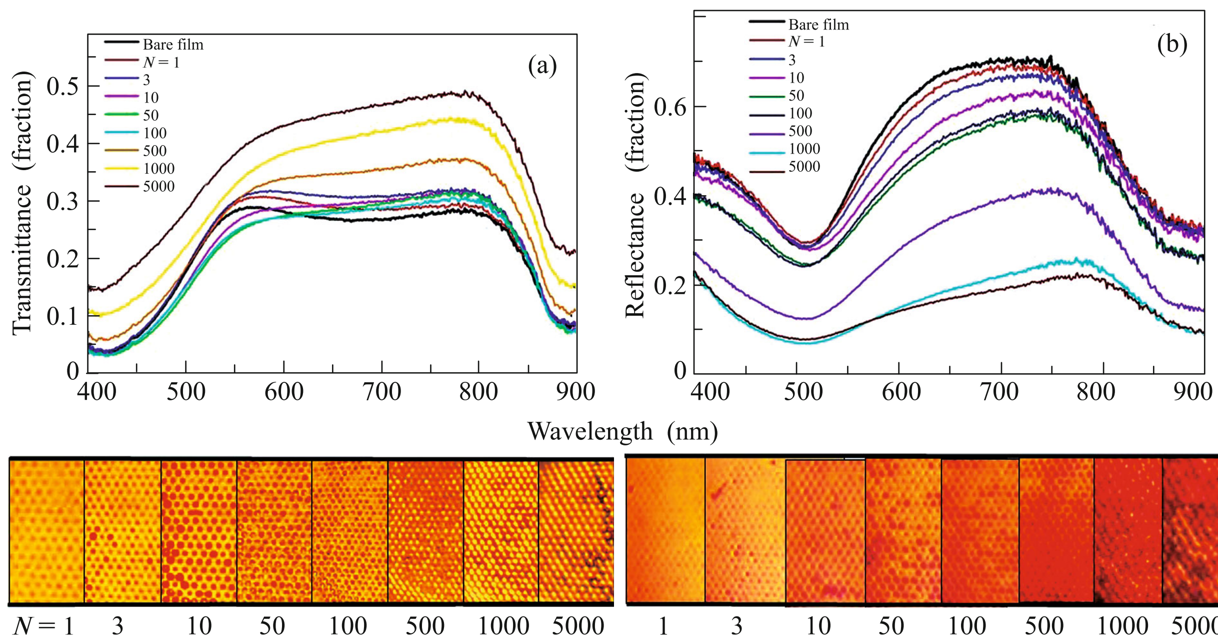

Fig. 4. (Color online) (a) Optical transmission spectra and (b) reflection spectra of arrays of nanoholes in an a-Si film 50 nm thick at different exposures N (indicated on the graphs); (bottom) optical microscopy images of these arrays at different exposures N in (left) transmission and (right) reflection.

nanoholes are filled with melt and dust, while the local hexagonal order of the modification regions is preserved, which points more likely to some internal causes of the destruction of nanoholes (possibly of plasmonic nature or due to random rescattering on the inhomogeneities of the structure), rather than to the instability of the interference pattern for mechanical reasons.

Similarly, the transmission and reflection spectra of arrays of nanoholes in the range of 400–900 nm (Fig. 4) demonstrate extremely weak changes in the corresponding coefficients at exposures $N < 500$ (slightly more pronounced for the reflection coefficient owing to the double pass of radiation through the structure), which points to the subwavelength nature of the holes and the superwavelength period of the

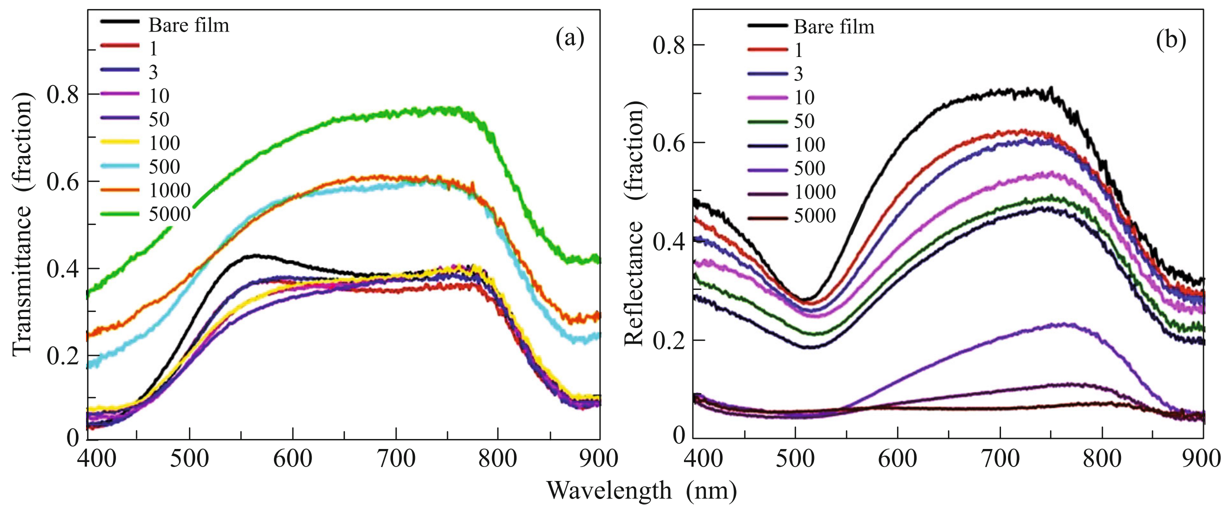

Fig. 5. (Color online) (a) Transmission and (b) reflection spectra of individual cells of nanohole arrays in an a-Si film 50 nm thick at different exposures N (indicated on the graphs).

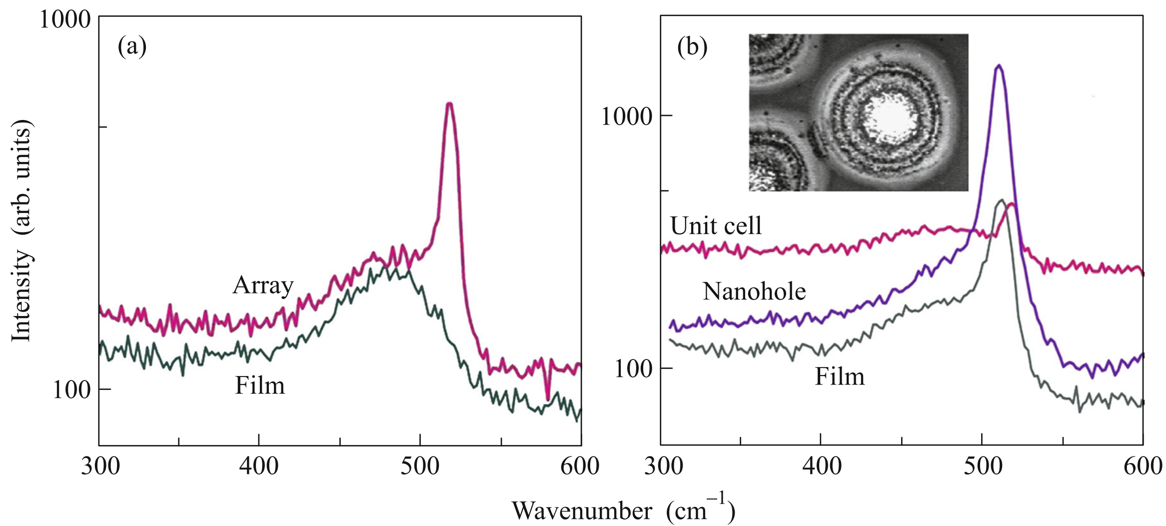

Fig. 6. (Color online) Raman spectra of the silicon (Film in (a)) outside the array of nanoholes, (Array) inside the array, (Unit cell) inside a unit cell, (Nanohole) inside nanohole, and (Film in (b)) on its periphery at the exposure of $N \approx$ (a) 100 and (b) 1000 pulses. Inset: a microscopy image of the inhomogeneous structure of nanoholes in the transmission (the distance between the centers of the holes is about 2 μm).

structure in this spectral range. At a higher exposure, $N > 500$, transmittance grows in the entire spectral region, whereas reflection drops, which can be associated with an increase in the diameter of the nanoholes (contrary to the SEM data in Fig. 3) and with annealing of the entire structure in the interference region, which removes the "tails" of absorption associated with defect states in the band gap of crystalline silicon (see the inset of Fig. 2b). Optical microscopy images of the arrays in the transmission and reflection modes clearly show the inversion of the color of the holes at $N > 500$ (Fig. 4).

A more detailed characterization of the transmission and reflection spectra of arrays of nanoholes in the range of 400–900 nm on the level of individual hexagonal cells reveals more noticeable changes in both the transmission and reflection coefficients while maintaining the same features of their spectra (Fig. 5).

The observed changes in the optical characteristics of nanohole arrays become clearer after analyzing the structure of the array material by Raman microscopy (Fig. 6). At exposure $N \approx 100$, a strong shifted peak of nanocrystalline silicon at (517.0 ± 0.3) cm^{-1}, having a half-width of about 11 cm^{-1} and a crystallite size of

about 3–5 nm, appears against the background of a wide band of amorphous silicon with a maximum in the region of 475 cm^{-1} (Fig. 6a) [16]. At higher exposures, $N \approx 1000$ (Fig. 6b), the peak of nanocrystalline silicon against the background of the band of amorphous material appears both on the images of the central region of the array (the size of the probed area is about 25 μm) and on the images of the material between the holes. Probing the complex ring-shaped structure of nanoholes obtained at high exposures shows a prominent peak of nanocrystalline silicon almost without any background signal of the amorphous material (Fig. 6b). The observed annealing of the film material in the region of formation of the array of nanoholes partly explains the above-discussed cumulative change in its optical characteristics as the laser exposure increases.

As follows from the above, multipulse interference femtosecond laser recording of arrays of subwavelength nanoholes in an amorphous silicon film with the use of a simple three-beam optical scheme allows fabricating multielement arrays of nanoholes with a size of up to 300 nm (despite a high rate of ambipolar diffusion in the dense electron–hole plasma at scales of 100–200 nm in a-Si [17]) with the preservation of regular packing of the modified areas of the film even after several thousand pulses, that is, with the preservation of long-term stability of the interference pattern; the contrast of the interference pattern is sufficient to avoid the formation of periodic surface nanostructures [13, 14]. Characterization in a broad spectral region (400–2000 nm) of an array formed at an exposure of $N \approx 50$ pulses shows that, in addition to the interference minimum in reflection near 500 nm (Figs. 4, 5), there is also a sharp minimum in the region of 1.2 μm (not shown), which is likely associated with the collective (diffraction) mode of the array. However, a strong exposure of $N \approx 1000$ pulses does not improve, but destroys arrays at the level of individual nanoholes, apparently, because of inhomogeneous annealing of the film material in the area of the interference and increasing intensity of scattered laser radiation on the inhomogeneous structure near the holes.

4. To summarize, we have studied the optical and structural processes in the formation of hexagonal arrays of nanoholes (metasurfaces) in a thin film of hydrogenated amorphous silicon by three-beam interference of multiplexed femtosecond laser pulses of the visible range at different exposures. The optimal mode of recording such arrays (metasurfaces) at intermediate laser exposures has been established and degradation of optical and structural characteristics of arrays at excessive exposure has been detected.

FUNDING

This work was supported by the Russian Science Foundation (project no.16-12-10165).

REFERENCES

1. M. J. A. de Dood, A. Polman, T. Zijlstra, and E. W. J. M. van der Drift, J. Appl. Phys. **92**, 649 (2002).
2. K. Narayanan and S. F. Preble, Opt. Express **18**, 8998 (2010).
3. K. Narayanan, A. W. Elshaari, and S. F. Preble, Opt. Express **18**, 9809 (2010).
4. M. R. Shcherbakov, P. P. Vabishchevich, A. S. Shorokhov, K. E. Chong, D. Y. Choi, I. Staude, A. E. Miroshnichenko, D. E. Neshev, A. A. Fedyanin, and Y. S. Kivshar, Nano Lett. **15**, 6985 (2015).
5. D. A. Zayarnyi, A. A. Ionin, I. V. Kiseleva, S. I. Kudryashov, S. V. Makarov, A. A. Rudenko, I. A. Timkin, R. A. Khmel'nitskii, and Ch. T. Kh. Nguen, JETP Lett. **100**, 295 (2014).
6. S. Syubaev, A. Zhizhchenko, A. Kuchmizhak, A. Porfirev, E. Pustovalov, O. Vitrik, Yu. Kulchin, S. Khonina, and S. Kudryashov, Opt. Express **25**, 10214 (2017).
7. S. I. Kudryashov, P. A. Danilov, A. P. Porfirev, I. N. Saraeva, T. H. T. Nguyen, A. A. Rudenko, R. A. Khmelnitskii, D. A. Zayarny, A. A. Ionin, A. A. Kuchmizhak, S. N. Khonina, and O. B. Vitrik, Appl. Surf. Sci. **484**, 948 (2019).
8. P. A. Danilov, D. A. Zayarny, A. A. Ionin, S. I. Kudryashov, A. A. Rudenko, A. A. Kuchmizhak, O. B. Vitrik, Yu. N. Kulchin, V. V. Zhakhovsky, and N. A. Inogamov, JETP Lett. **104**, 759 (2016).
9. I. Shishkin, A. Polushkin, E. Tiguntseva, A. Murzin, B. Stroganov, Y. Kapitonov, S. Kulinich, A. Kuchmizhak, and S. Makarov, Appl. Phys. Express **12**, 122001 (2019). https://doi.org/10.7567/1882-0786/ab4b1b
10. P. A. Danilov, D. A. Zayarny, A. A. Ionin, S. I. Kudryashov, E. P. Litovko, N. N. Mel'nik, A. A. Rudenko, I. N. Saraeva, S. F. Umanskaya, and R. A. Khmel'nitskii, JETP Lett. **105**, 727 (2017).
11. S. Makarov, S. I. Kudryashov, I. Mukhin, A. Mozharov, V. Milichko, A. Krasnok, and P. A. Belov, Nano Lett. **15**, 6187 (2015).
12. N. A. Smirnov, S. I. Kudryashov, P. A. Danilov, A. A. Rudenko, A. A. Ionin, and A. A. Nastulyavichus, JETP Lett. **108**, 368 (2018).
13. D. V. Amasev, M. V. Khenkin, R. Drevinskas, P. Kazansky, and A. G. Kazanskii, Tech. Phys. **62**, 925 (2017).
14. D. V. Shuleiko, F. V. Potemkin, I. A. Romanov, I. N. Parhomenko, A. V. Pavlikov, D. E. Presnov, S. V. Zabotnov, A. G. Kazanskii, and P. K. Kashkarov, Laser Phys. Lett. **15**, 056001 (2018).
15. Z. Zeng, Q. Zeng, W. L. Mao, and S. Qu, J. Appl. Phys. **115**, 103514 (2014).
16. G. Faraci, S. Gibilisco, P. Russo, A. R. Pennisi, and S. La Rosa, Phys. Rev. B **73**, 033307 (2006).
17. P. Danilov, A. Ionin, R. Khmelnitskii, I. Kiseleva, S. Kudryashov, N. Melnik, A. Rudenko, N. Smirnov, and D. Zayarny, Appl. Surf. Sci. **425**, 170 (2017).

Translated by V. Alekseev